Investigation of Electrochemically Mediated Atom Transfer Radical Polymerization

ARTICLE *in* MACROMOLECULES · MAY 2013

Impact Factor: 5.8 · DOI: 10.1021/ma400869e

6 AUTHORS, INCLUDING:

Andrew Magenau
Drexel University
22 PUBLICATIONS **756** CITATIONS
SEE PROFILE

Nicola Bortolamei
University of Padova
8 PUBLICATIONS **223** CITATIONS
SEE PROFILE

Elena Frick
Karlsruhe Institute of Technology
6 PUBLICATIONS **81** CITATIONS
SEE PROFILE

Armando Gennaro
University of Padova
107 PUBLICATIONS **2,793** CITATIONS
SEE PROFILE

Macromolecules

Article

pubs.acs.org/Macromolecules

Investigation of Electrochemically Mediated Atom Transfer Radical Polymerization

Andrew J. D. Magenau,[†] Nicola Bortolamei,[‡] Elena Frick,[†] Sangwoo Park,[†] Armando Gennaro,[‡] and Krzysztof Matyjaszewski*[,†]

[†]Department of Chemistry, Carnegie Mellon University, 4400 Fifth Avenue, Pittsburgh, Pennsylvania 15213, United States

[‡]Dipartimento di Scienze Chimiche, Università di Padova, Via Marzolo 1, Padova 35131, Italy

Supporting Information

ABSTRACT: Electrochemically mediated atom transfer radical polymerization (*e*ATRP) of *n*-butyl acrylate was systematically investigated using diminished catalyst concentrations (≤300 parts per million) under a variety of formulations and electrochemical conditions. Critical polymerization parameters, including the applied potential, catalyst concentration, and ligand, were explored and correlated with polymerization rates, polymer properties, and currents during the *e*ATRP process. Additional electrochemical methods were explored to improve the feasibility of *e*ATRP under galvanostatic conditions. Copper electrodeposition and stripping experimentation proved to be an effective strategy for catalyst recycling allowing sequential controlled polymerizations to be possible utilizing one catalyst charge.

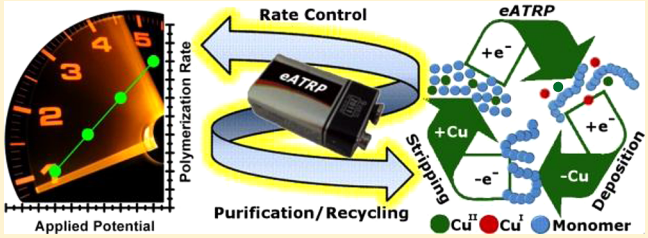

INTRODUCTION

Controlled/living radical polymerization (CRP) provides macromolecules of uniform size, predetermined molecular weight, and with retained chain-end functionality.[1] Radical polymerization processes of this category are amenable to a vast array of monomer classes (e.g., styrenes, (meth)acrylates, (meth)acrylamides, or vinyl esters), reagents, functional groups, reaction conditions, and allow specific and defined placement of various functionalities. Owing to these characteristics, CRP processes provide exquisite control of macromolecules by granting access to more complex compositions (i.e., block, gradient, statistical copolymers) and complex polymeric architectures, exemplified by star, cyclic, brush, hybrid (i.e., bioconjugate, inorganic/organic), and network-type structures. Furthermore, the versatility of these systems permits them to be performed in disparate polymerization media, ranging from homogeneous organic and aqueous systems to heterogeneous emulsions and suspension systems. Of the existing CRP techniques, the most powerful and commonly employed systems include reversible addition−fragmentation chain transfer (RAFT),[2] nitroxide-mediated polymerization (NMP),[3] organometallic-mediated radical polymerization (OMRP),[4] and atom transfer radical polymerization (ATRP).[5]

ATRP functions through a catalytic process mediated by redox-active transition metal complexes (Mt/L: Mt = Cu, Ru, Fe, Mo, Os, etc., L = ligand),[6] forming a dynamic equilibrium between dormant species (alkyl halide initiator: R−X and polymer: P_n−X) and active propagating radicals ($P_n^\bullet$).[5a] This equilibrium essentially mediates the polymerization, providing a constant [$P_n^\bullet$], and ensures concurrent growth of all polymer chains. In the dormant state, a lower oxidation state catalyst (Cu^IL^+)[7] reduces P_n−X to intermittently generate $P_n^\bullet$ and its corresponding higher oxidation state catalyst (X−$Cu^{II}L^+$). In the active state, $P_n^\bullet$ can temporarily propagate with monomer (M), terminate, or be deactivated with X−$Cu^{II}L^+$ at rates proportional to their respective rate coefficients (k_p, k_t, and k_{da}, respectively) and involved reagent concentrations. The ATRP equilibrium (K_{ATRP}), formally defined as the ratio of activation (k_a) and deactivation (k_{da}) rate coefficients, spans values over ca. 10^8, which can be tuned by the employed reagent structures (i.e., alkyl halide and catalyst)[6,8] and reaction conditions (i.e., temperature, pressure, and solvent).[9] These various system parameters can be used to optimize and tune the polymerization rate (R_p) and polymer dispersity (M_w/M_n) as dictated by eqs 1 and 2, where *p* and DP represent monomer conversion and the degree of polymerization, respectively.

$$R_p = k_p[P_n^\bullet][M] = \left(\frac{k_p k_a[R{-}X]_0[Cu^IL^+]}{k_{da}[X{-}Cu^{II}L^+]}\right)[M] \quad (1)$$

$$\frac{M_w}{M_n} = 1 + \frac{1}{DP} + \left(\frac{k_p([R{-}X]_0)}{k_{da}[X{-}Cu^{II}L^+]}\right)\left(\frac{2}{p} - 1\right) \quad (2)$$

During the past decade, ATRP has become more universal in application because of several key advancements and its fusion with many externally applied stimuli. One significant improvement was the advent of activators regenerated by electron

Received: April 28, 2013
Revised: May 14, 2013
Published: May 28, 2013

transfer (ARGET)[10] and related processes,[11] which achieved parts per million (ppm) catalyst loadings, tolerance to O_2,[12] and diminished side reactions,[13] while maintaining all the traditional attributes of ATRP/CRP. In ARGET type systems, the activator complex is continuously (re)generated by a reducing agent (e.g., Sn^{II}, ascorbic acid, free radical initiator, cathodic current, or light) from otherwise accumulated X–$Cu^{II}L^+$ originating from unavoidable radical termination events. In addition to these advancements, the ATRP process can be manipulated by a variety of stimuli including, but not limited to, pressure,[14] light,[15] and electrical current.[12c,16] Applied stimuli provide additional features and control to the ATRP process by enabling the synthesis of high molecular weight polymers,[14b] local/temporal catalyst activation, and "on-demand" catalyst manipulation.[15d,16a] Electrochemically mediated ATRP (*e*ATRP), the newest member of the ATRP family, utilizes both the concept/advantages of ARGET ATRP via an electrochemical stimulus (Scheme 1) to provide enhanced levels of polymerization control.

Scheme 1. Electrochemically Mediated ATRP (*e*ATRP)

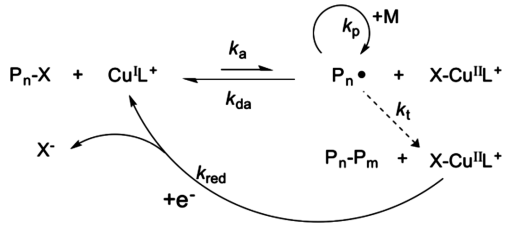

Electrochemical methods and reagents are emerging as an ever more powerful tool in polymer science in regard to catalyst characterization,[8a,17] catalyst (re)generation,[18] redox responsive materials,[17b,19] and surface chemistries.[12c,18a,20] In ATRP alone, electrochemistry has been critical as a characterization method to determine equilibrium,[8a] ligand binding,[21] and activation rate coefficients.[7,22] In other polymerization systems, catalyst activity was manipulated by utilization of redox-sensitive catalysts in the polymerization of lactide.[23] From a materials perspective, redox-sensitive polymer materials have been developed including well-defined ferrocene containing (meth)-acrylate polymers[19a] and electropatterned surface brushes.[12c] In regard to catalyst generation and electropolymer synthesis, *e*ATRP was recently developed as a tool to effectively synthesize well-defined polymers by mediating ATRP through passage of current. Enhanced levels of polymerization control were realized via electrochemical means by generating the active catalyst *in situ* through electrolysis. Control of the polymerization rate and ability to intermittently switch a polymerization between "on" and "off" states were demonstrated.[16a] The utility of *e*ATRP was further extended to aqueous/buffered media, typically challenging in ATRP, to produce well-defined polymers by tuning relative catalyst concentrations via the applied potential (E_{app}).[16b] Most recently, the *e*ATRP process has been extended to surface-initiated polymerizations providing controlled and tailorable growth of polymer brushes under ambient conditions, while enabling multiple surface functionalizations by recycling/reusing the reaction medium.[12c]

To promote widespread application of *e*ATRP, this work serves to provide an in-depth investigation and extension of our first report, disseminating practical insight into fundamental polymerization parameters, simplified reaction setups, and an extension of this process as an efficient purification and catalyst recycling tool. Variable electrochemical methods were explored, and polymerization parameters were investigated, including the applied potential, catalyst type and loading, galvanostatic conditions, and electrodeposition/stripping experiments.

RESULTS AND DISCUSSION

Characterization and Control Studies. All experimentation presented in this work was conducted in a two-compartment electrochemical cell equipped with a platinum disk and platinum mesh working electrode, platinum plate counter electrode, and Ag|AgI|I^- reference electrode[24] maintained under an inert N_2 atmosphere. Prior to each polymerization, cyclic voltammetry (CV) was used to verify the existence of the redox active catalyst and to identify appropriate potentials to manipulate its oxidation state. Figure 1 represents

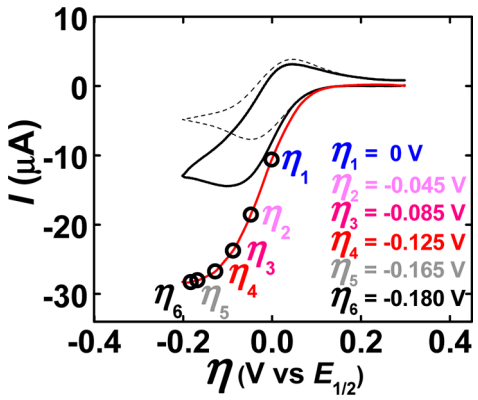

Figure 1. CV of 1.17 mM Br–Cu^{II}TPMA$^+$ in 56% (v/v) BA/DMF ($[BA]_0$ = 3.9 M) containing 0.2 M $TBAClO_4$ recorded at a scan rate (ν) of 50 mV/s in the absence (dashed black) and presence (solid black) of 12.9 mM EB*i*B. LSV (solid red) using an identical formulation to those in CV containing EB*i*B under convection. Hollow black dots correspond to applied potential values (E_{app}), expressed as overpotential (η) values, used in subsequent *e*ATRP experiments. $E_{1/2}$ values of 0.322 and −0.166 V were determined using Ag|AgI|I^- and SCE, respectively.

a summary of two CVs and one linear sweep voltammogram (LSV) conducted in a polymerization mixture prior to electrolysis/polymerization. The polymerization medium was composed of a solution of monomer, *n*-butyl acrylate (BA), in solvent, dimethylformamide (DMF), containing a supporting electrolyte, tetrabutylammonium perchlorate ($TBAClO_4$). Initial *e*ATRP experiments utilized a catalytic system of Cu^{II}/tris(2-pyridylmethyl)amine (Br–Cu^{II}TPMA$^+$) and later involving different ligands to including tris[2-(dimethylamino)ethyl]-amine (Me_6TREN) and *N*,*N*,*N*′,*N*″,*N*″-pentamethyldiethylene-triamine (PMDETA). In all cases, equimolar concentrations of copper(II) and bromide were utilized by adding copper(II) trifluoromethanesulfonate ($Cu^{II}OTf_2$) and tetrabutylammonium bromide (TBABr), respectively. For clarity, the [TBABr] has been omitted from figures and captions. Specific formulation details are supplied in the figure footnotes and Supporting Information. As expected, a typical copper redox couple of Br–Cu^{II}TPMA$^+$ was observed having quasi-reversible behavior with a half-wave potential ($E_{1/2}$) value of 0.322 V vs Ag|AgI|I^-. For further reference, CVs were recorded against the saturated calomel electrode (SCE) which gave an $E_{1/2}$ of

dx.doi.org/10.1021/ma400869e | *Macromolecules* 2013, 46, 4346–4353

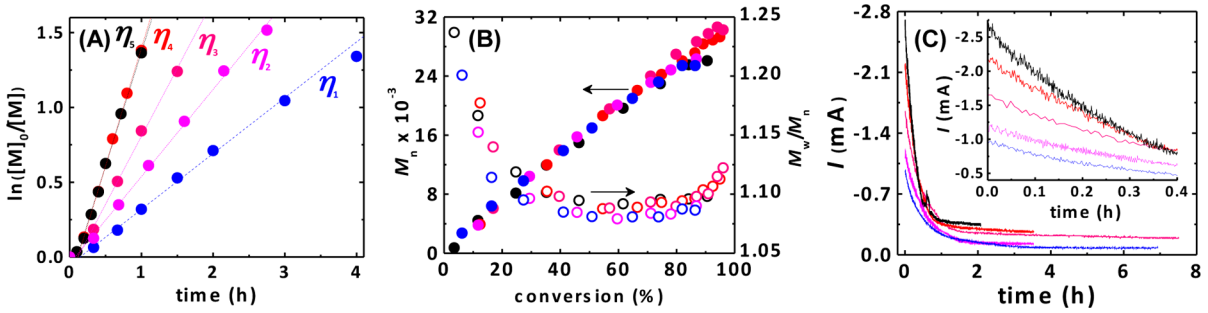

Figure 2. Kinetics of *e*ATRP as a function of E_{app} at a η ranging from 0 to −0.165 V. (A) First-order plot of monomer conversion versus time, (B) M_n and M_w/M_n versus conversion, and (C) current versus time. Reaction conditions: $[BA]_0/[EBiB]_0/[Br-Cu^{II}TPMA^+]_0$ = 300/1/0.09, $[TBAClO_4]_0$ = 0.2 M, $[BA]_0$ = 3.9 M in DMF, T = 44 °C, V_{tot} = 23 mL, and stirring rate (f) = 875 rpm. For clarity η_6 = −0.180 V was omitted from (A), (B), and (C).

−0.166 V vs SCE. In each case, the anodic and cathodic peaks were separated by ca. 80 mV under fully compensated conditions (dashed black line). All following discussions and figures will report applied potential values as overpotential (η) values, formally defined as the difference between the applied potential (E_{app}) and $E_{1/2}$, unless otherwise stated in the following discussion ($\eta = E_{app} - E_{1/2}$).

Once the $E_{1/2}$ value was determined, an alkyl halide initiator (ethyl α-bromoisobutyrate, EB*i*B) was injected into the working solution, causing a change in the CV shape (solid black line). Similar to previous literature accounts,[16] an increase in the cathodic current and decrease in the anodic current were observed, verifying the presence of an additional homogeneous chemical reaction.[25] In the presence of R−X, a catalytic electrochemical−chemical (EC′) reaction[26] occurred where the electrochemically generated Cu^IL^+ reacted with R−X regenerating $Br-Cu^{II}L^+$ and depleting Cu^IL^+ near the electrode surface (cf. Scheme S1). LSV was next conducted to estimate potential values where limiting current/mass transport conditions existed under convection (i.e., stirring, solid red line). Three regions were observed: (1) the onset of $Br-Cu^{II}L^+$ reduction near 0.075 V, (2) an increase in cathodic current with potential, and (3) a limiting current region at diffusion controlled conditions near ca. −0.117 V. This LSV indicates a point where no further reduction rate enhancement is possible even after application of increasingly more negative potentials, providing insight into the potential range to study for our later E_{app} (i.e., η) analysis.

Before conducting *e*ATRP, control bulk electrolysis reactions were carried out in the absence of R−X (at both η = 0 and −165 mV) to evaluate the electrochemical contribution of $Br-Cu^{II}L^+$ and to confirm the absence of any polymerization. In the limiting current regime, a η value of −165 mV was applied to ensure near-quantitative conversion of $Br-Cu^{II}L^+$ to Cu^IL^+ in the vicinity of the electrode and reaction mixture. Under these conditions, the current efficiency (CE) and maximum apparent reduction rate coefficient (k_{red}) can be estimated for $Br-Cu^{II}L^+$. A cathodic current resulted initially of ca. −3 mA which absolute value decreased in an exponential fashion to a nominal and constant value of ca. −70 μA (Figure S1a, black trace). Assuming complete conversion of $Br-Cu^{II}L^+$, the theoretical total charge passed (Q_{theo}) should equal 2.61 C based upon a single electron reduction and a system containing 2.7×10^{-5} mol of $Br-Cu^{II}L^+$. After performing the electrolysis, the charge passed (Q_{exp}) was determined to be 2.85 C after 4500 s, which is slightly larger than the Q_{theo} equal to 2.61 C. This corresponds to a CE of ca. 92%, implying a small fraction of charge is lost to other reduction processes or due to the presence of O_2. However, if the charge passed due to the nominal current is subtracted from the total charge passed, a new Q_{exp} value of 2.53 C can be obtained, which is nearly identical to Q_{theo}. Furthermore, in the absence of R−X, there is no homogeneous contribution and loss of Cu^IL^+, and therefore, the system can be treated as a first-order homogeneous chemical reaction. When the applied potential is in the limiting current regime, a linear relationship existed, corresponding to a maximum $Br-Cu^{II}L^+$ k_{red} of 1×10^{-3} s^{-1}, whereas at η = 0 V the apparent reduction rate coefficient was found to be 4.4×10^{-4} s^{-1} (Figure S1b). This maximum k_{red} value was found to be in close proximity to the k_{red} obtained in an identical polymerization system containing R−X (Figure S2). Because of this similarity, k_{red} values in *e*ATRP may be estimated under these specific conditions to be between 1×10^{-3} and 4.4×10^{-4} s^{-1}. As a side note, each control electrolysis experiment proceeded without polymerization, as confirmed by gel permeation chromatography (GPC) and nuclear magnetic resonance (NMR).

Influence of Applied Potential/Overpotential. After establishment of the system behavior without alkyl halide, a series of polymerizations were carried out with R−X to examine the influence of η on the polymerization behavior. It is well known that electrode potentials strongly affect the kinetics of reactions occurring on its surface, and in *e*ATRP they would dictate the relative $[Cu^IL^+]$ and $[Br-Cu^{II}L^+]$ within the polymerization mixture. It should be stressed that electrochemical systems like *e*ATRP are heterogeneous in nature and may have different catalyst concentrations in areas near the electrode surface compared to the working solution. Initial scouting experiments revealed that stirring was required during *e*ATRP; otherwise, under stagnant conditions, passivation of the working electrode occurred along with a slow R_p and polymers with large dispersity values ($M_w/M_n \geq 2.0$), as shown in Figure S3. Our previous reports demonstrated that *e*ATRP was capable of modulating the rate of polymerization;[16a] however, the limits of this behavior have yet to be established.

Figure 2 summarizes the results of five polymerizations conducted at a broad range of η values spanning over 180 mV beginning from the $E_{1/2}$ at η_1 = 0 V to η_6 = −0.180 V. Figure 2A is a first-order kinetic plot of the resulting five polymerizations, each conducted with identical formulations but with increasingly more negative applied potentials (cf. Figure 1 for η values). For each polymerization, linear first-order kinetic behavior was observed until ca. 80% monomer conversion. Increasingly more negative η values provided larger apparent rate coefficients (k_{app}). A k_{app} of 0.37 and 1.58 h^{-1} resulted

dx.doi.org/10.1021/ma400869e | *Macromolecules* 2013, 46, 4346−4353

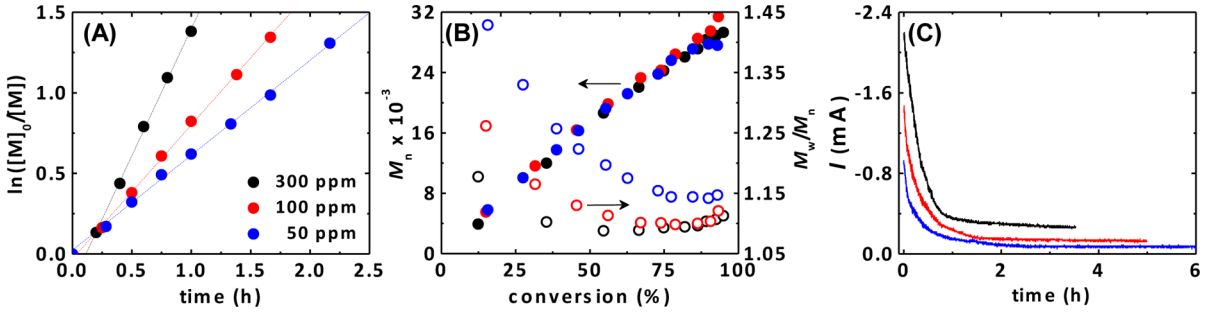

Figure 3. *e*ATRP as a function of $[Br-Cu^{II}L^+]_0$ with a $\eta_4 = -0.125$ V. (A) First-order kinetic plot of monomer consumption, (B) M_n and M_w/M_n versus conversion, and (C) current versus time. Reaction conditions: $[BA]_0/[EBiB]_0/[Br-Cu^{II}TPMA^+]_0 = 300/1/X$, $[TBAClO_4]_0 = 0.2$ M, $[BA]_0 = 3.9$ M in DMF, $T = 44$ °C, $V_{tot} = 23$ mL, and $f = 875$ rpm. $X = 0.9$, 0.3, and 0.15 corresponding to 300, 100, and 50 ppm, respectively.

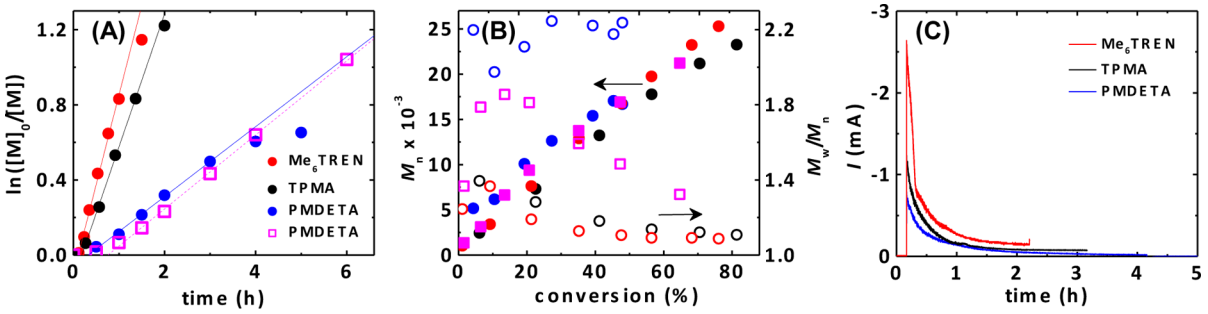

Figure 4. *e*ATRP as a function of ligand (L = Me_6TREN, TPMA, and PMDETA) with a $\eta = -0.180$ V and 100 ppm catalyst. Note: the second instance of PMDETA (magenta squares) was conducted instead with a $\eta = -0.125$ V and 300 ppm catalyst. (A) First-order kinetic plot of monomer conversion versus time, (B) M_n and M_w/M_n versus conversion, and (C) current versus time. Reaction conditions: $[BA]_0/[EBiB]_0/[Br-Cu^{II}L^+]_0 = 300/1/0.03$, $[TBAClO_4]_0 = 0.2$ M, $[BA]_0 = 3.9$ M in DMF, $T = 44$ °C, $V_{tot} = 23$ mL, and $f = 875$ rpm.

when using η of 0 and −0.165 V, respectively, providing a 4-fold enhancement in the R_p. This increase in k_{app} was synonymous in magnitude with the 4-fold enhancement of k_{red}, when applying the same η values, confirming a correlation exists between the polymerization rate and reduction rate (i.e., current). However, a limiting region existed between $\eta = -0.125$ and −0.165 V, where minimal change in the k_{app} was observed even with application of progressively more negative potentials (η_4–η_5) due to mass transport limitations. One additional polymerization was conducted at $\eta_6 = -0.180$ V, confirming the k_{app} limit of 1.58 h^{-1} found for $\eta_5 = -0.165$ V. For convenience, a semilogarithmic plot of the observed k_{app} versus η values (Figure S4) is supplied, illustrating the potential "dependent" and "independent" regimes of the η on the k_{app}.

The resulting number-average molecular weight (M_n) and M_w/M_n values are provided in Figure 2B. Controlled polymerization behavior was confirmed in all cases by the linear increase of M_n with conversion, while producing a monomodal population of polymers with relatively low M_w/M_n values, approaching ca. 1.10. Slightly lower M_w/M_n values were observed for systems operating at more positive potential values owing to a larger $[Br-Cu^{II}L^+]$.

During each polymerization, the resulting current was recorded as shown in Figure 2C. In the early stages of polymerization, high current values were observed representing the original generation of Cu^IL^+ from a purely $Cu^{II}L^+$ system to initiate polymerization. Here the concentrations of Cu^IL^+ and $Br-Cu^{II}L^+$ are dynamic. After this stage, the current becomes fairly constant resembling the point where equilibrium is reached and a constant concentration of $Br-Cu^{II}L^+$ and Cu^IL^+ exist. More negative η values produced larger initial currents, indicative of a faster rate of reduction, and larger stationary current values. In essence, faster rates of reduction provide a higher $[Cu^IL^+]$ and, therefore, faster polymerizations originating from a higher $[P_n^\bullet]$. The magnitude of stationary current values, after ca. 1 h, reflect the relative Cu^IL^+ regeneration rates and hence terminate rates; i.e., a more negative η equals a higher R_p and stationary current, resulting in more termination.

Influence of $[Br-Cu^{II}L^+]_0$. The next series of polymerizations were designed to probe the influence of the concentration of electroactive species within *e*ATRP. Three polymerizations were conducted using $[Br-Cu^{II}L^+]_0$ ranging from 300 to 50 ppm catalyst loadings, as shown in Figure 3A–C. In these experiments, identical E_{app} values at $\eta_4 = -0.125$ V were employed.

Figure 3A shows three polymerizations displaying first-order kinetic behavior as a function of the $[Br-Cu^{II}L^+]_0$. As the $[Br-Cu^{II}L^+]_0$ increases, the rate of polymerization increases with a near square root dependence, similar to other literature accounts which display larger rates with higher catalyst loadings.[11d,27] A larger R_p reflects a higher $[P_n^\bullet]$, a result of faster reduction rates generating more Cu^IL^+. Figure 3B illustrates, in all cases, a linear increase in M_n with respect to conversion and a profound decreases in the relative M_w/M_n values with larger $[Br-Cu^{II}L^+]_0$. This observation is supported by eq 2, where larger $[Br-Cu^{II}L^+]$ should produce polymers with lower M_w/M_n values from an increased rate of deactivation and fewer monomer additions within each activation–deactivation cycle. The current profiles (Figure 3C) further support the relative concentration of $Br-Cu^{II}L^+$ in the system, inferred via the Cottrell equation,[26a] where the largest current values were obtained with the largest concentration of electroactive species. Furthermore, the steady state current

dx.doi.org/10.1021/ma400869e | *Macromolecules* 2013, 46, 4346–4353

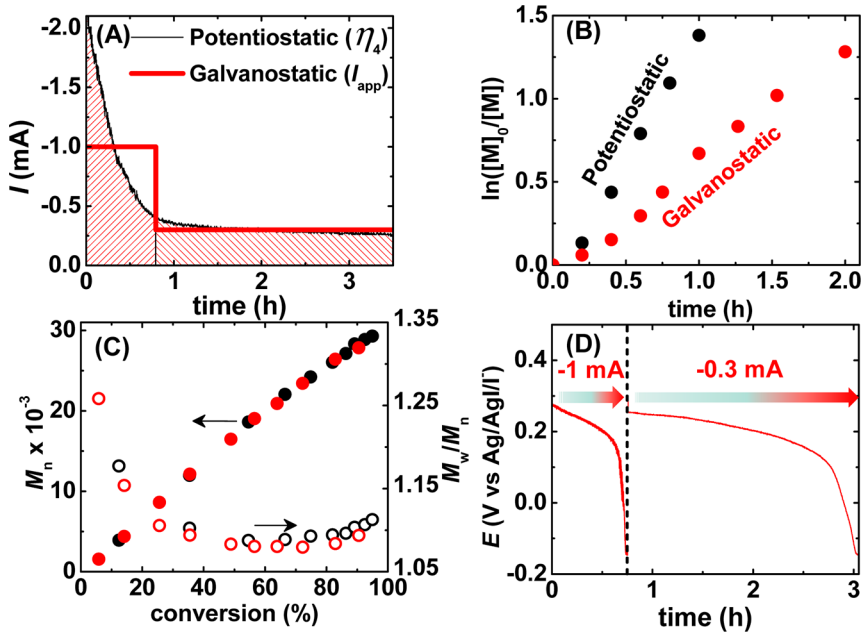

Figure 5. Galvanostatic versus potentiostatic *e*ATRP. (A) Current versus time for a potentiostatic polymerization (black) using an E_{app} at a η_4 = −0.125 V and galvanostatic polymerization (red) using an I_{app} of −1 mA (t = 2800 s) and −0.3 mA (t = 9800 s). Red hashes represent integrated area to calculate Q for current determination. (B) First-order kinetic plot of a potentiostatic and galvanostatic *e*ATRP. (C) M_n and M_w/M_n versus conversion for potentiostatic (black) and galvanostatic (red) *e*ATRP. (D) Monitored applied potential versus time during a galvanostatic *e*ATRP. Reaction conditions: $[BA]_0/[EBiB]_0/[Br-Cu^{II}TPMA^+]_0$ = 300/1/0.09, $[TBAClO_4]_0$ = 0.2 M, $[BA]_0$ = 3.9 M in DMF, T = 44 °C, V_{tot} = 23 mL, and f = 875 rpm.

values (at time >2 h) imply larger Cu^IL^+ regeneration rates with larger $[Br-Cu^{II}L^+]$.[28]

Influence of Ligand Structure. The next series of polymerizations were designed to probe the influence of different catalytic systems within *e*ATRP at 100 ppm catalyst and to demonstrate the ability to gain CRP behavior in otherwise uncontrolled conditions. Three different ligands were selected, to including Me_6TREN, TPMA, and PMDETA, and electrolysis experiments were performed at relatively equal η values of −0.125 V. CVs pertaining to each complex are supplied in the Supporting Information (Figure S5) against AgI|AgI‖I$^-$, conducted in the absence and presence of EB*i*B. Consistent with previous reports, the $E_{1/2}$ values became gradually more negative, signifying larger K_{ATRP} values, moving from PMDETA to TPMA to Me_6TREN.[8a] Furthermore, increased catalytic behavior, i.e., a larger cathodic current, was realized with progressive more active ligands (PMDETA < TPMA < Me_6TREN) when in the presence of EB*i*B.

As shown in Figure 4A, the R_p is heavily dependent on the ligand selection. Progressively more active ligands provide faster rates of polymerization from larger K_{ATRP} values. Furthermore, as shown in Figure 4B, more active ligands (i.e., Me_6TREN and TPMA) provided lower M_w/M_n values at identical $[Br-Cu^{II}L^+]_0$, whereas PMDETA (blue symbols) had M_w/M_n values of ca. 2.2. Similar to ARGET ATRP, more active catalysts are capable of maintaining sufficient rates of deactivation, minimizing relative M_w/M_n values.[10a] Further to this point, the high activity catalysts were capable of achieving conversion values ≥80%, whereby PMDETA was limited to 50%. When employing lower activity catalysts (i.e., with PMDETA), *e*ATRP provides two parameters to reduce the M_w/M_n by using a larger $[Br-Cu^{II}L^+]_0$ and/or a more positive η value, each essentially increasing the effective $[Br-Cu^{II}L^+]$ in the reaction medium. After increasing the catalyst loading to 300 ppm and using a more positive η_4 of −0.125 V, the M_w/M_n value could be decreased to ca. 1.3, while concomitantly providing higher conversion values (magenta squares). The current profiles, shown in Figure 4C, reveal that more active catalysts result in larger initial and stationary current values.

Galvanostatic *e*ATRP. In an effort to improve the feasibility of *e*ATRP, for both academic and industrial research, a galvanostatic *e*ATRP was investigated. When using galvanostatic conditions, i.e., a constant current instead of a constant potential, the reference electrode can be eliminated, and therefore, *e*ATRP can be conducted using a two-electrode system. In order to carry out a galvanostatic *e*ATRP, appropriate current values must be selected which can be rationalized from previously conducted potentiostatic experiments. Polymerization conditions were selected to be identical to those utilized in our applied potential studies (Figure 2, η_4), except by employing a constant current. For convenience, our selected current values (thick red line) were superimposed over the current profile of a previously conducted potentiostatic polymerization (black line), as shown in Figure 5A. The selected current values were determined by integration of this current profile, the area designated by red hashes, to determine the Q passed during the course of a potentiostatic *e*ATRP. The selected current values resembled those of the potentiostatic polymerization, whereby an initial high current value (i.e., I_{app} = −1 mA for 2800 s) and consecutive low current value (i.e., I_{app} = −0.3 mA for 9800 s) were employed. This two-stage current program was hypothesized to rapidly convert the vast majority of $Br-Cu^{II}L^+$ to Cu^IL^+, initiating *e*ATRP, and next providing compensation for any (re)generated $Br-Cu^{II}L^+$ incurred from termination.

Figure 5B provides a comparison of the polymerization kinetics in both potentiostatic and galvanostatic mode. The galvanostatic polymerization proceeded at a slower rate. A

dx.doi.org/10.1021/ma400869e | *Macromolecules* 2013, 46, 4346−4353

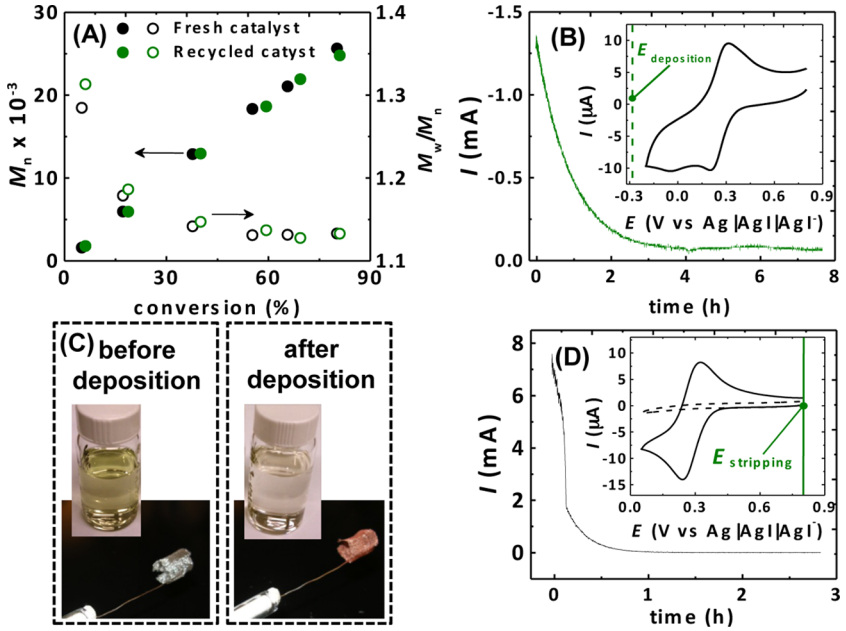

Figure 6. Recycling of copper via electrodeposition and stripping for sequential *e*ATRP polymerizations. (A) M_n and M_w/M_n versus conversion for fresh (black) and recycled (green) catalyst. (B) Current versus time plot during copper deposition with an E_{app} at −0.283 V vs Ag|AgI|I⁻ (inset: CV after first polymerization conducted with v = 250 mV/s and T = 65 °C). (C) Images of crude polymerization mixture and Pt working electrode, before and after deposition. (D) Current versus time during copper stripping with an E_{app} at 0.800 V vs Ag|AgI|I⁻ (inset: CV before (dashed line) and after (solid line) copper stripping). Reaction conditions: $[BA]_0/[EBiB]_0/[Br-Cu^{II}TPMA^+]_0$ = 300/1/0.09, $[TBAClO_4]_0$ = 0.2 M, $[BA]_0$ = 3.9 M in DMF, T = 44 °C, V_{tot} = 23 mL, η_6 = −0.180 V, and f = 875 rpm.

lower R_p was expected as a lower stationary current (−1 mA) was imparted in comparison to values as high as −2 mA in potentiostatic mode. Regardless, the resulting polymers from both techniques confirmed controlled polymerizations took place providing polymers with low M_w/M_n values (Figure 5C). Although a reference electrode was not necessary, the potential at the working electrode was monitored using an Ag|AgI|I⁻ reference electrode to gain insight into the behavior of a galvanostatic *e*ATRP (Figure 5D). The working electrode potential was observed to be maintained at approximately the $E_{1/2}$ of (Cu^{II}TPMA|Cu^{I}TPMA) or at slightly more negative values. However, at later portions of each current stage, the observed potential progressively became more negative to satisfy the current requirements and/or from an increased solution resistivity due to higher solution viscosities. If the applied current values were maintained for longer durations, more negative potentials would have resulted, leading to substantial copper deposition on the working electrode.

Catalyst Recycling: Deposition and Stripping. One distinct advantage of an electrochemical process is the diversity of techniques which can be conducted. Owing to this diversity, electrochemical deposition and stripping techniques were employed to recycle the copper catalyst (i.e., solely the metal center) for two separate and sequential polymerizations. To begin, a polymerization was conducted using previously established conditions with TPMA and 300 ppm of copper, as reported in Figure 2 at a η_6 = −0.180 V. As expected a controlled polymerization occurred resulting in well-defined polymers with narrow M_w/M_n values (Figure 6A, black dots). The CV prior to polymerization and the first-order kinetic plot are shown in Figure S6 (black traces).

After the first *e*ATRP was completed, the temperature of the reactor was increased to 65 °C and an E_{app} (deposition) of −0.283 V vs Ag|AgI|I⁻ was utilized. This potential value is approximately 570 mV more negative than the $Cu^{II}L/Cu^{I}L$ couple and nearly 300 mV more negative than that of the Cu^0 deposition peak, located at ca. −45 mV vs Ag|AgI|I⁻ (Figure 6B, inset). These conditions were selected based upon optimization experiments for electrodeposition of copper onto the working electrode. When conducting preliminary CV analysis as a function of temperature, the cathodic peak associated with conversion of Cu^I to Cu^0 shifted to more positive values by nearly 430 mV vs Ag|AgI|I⁻ upon increasing the reaction temperature from 25 to 60 °C (Figure S8A). These results confirmed that higher temperatures favored the formation of Cu^0 on the working electrode. With this in mind, copper deposition was performed at a higher reaction temperature of 65 °C. After application of E_{app} (deposition), the resulting current profile (green line), given in Figure 6B, decreased, indicating depletion of any soluble copper species in the reaction medium. The copper deposition process required nearly 4 h to reach nominal current values of ca. −70 μA and was allowed to proceed for a total of 8 h. GPC was conducted before (M_n = 25 100 and M_w/M_n = 1.08) and after deposition (M_n = 28 300 and M_w/M_n = 1.11), confirming a minimal change in the resulting polymer which was accompanied by an increase of monomer conversion from 80 to 94%. A UV−vis calibration curve was generated to determine the concentration of copper before and after deposition (Figure S8B). The initial and resulting copper concentrations were found to be 1.18 and 0.05 mM, respectively, indicating over 95% of the Cu was removed from the reaction mixture. Visual confirmation of the copper deposition can be seen in Figure 6C, both in the working solution (i.e., clear green to clear light yellow solution) and on the working electrode (platinum to metallic copper in appearance).

After collecting essentially all the copper as metallic copper on the working electrode, this copper-coated electrode was

dx.doi.org/10.1021/ma400869e | *Macromolecules* 2013, 46, 4346−4353

directly submerged into another fresh polymerization mixture containing all reagents except for Cu^{II}. Prior to stripping, a CV was recorded (Figure 6D, inset (dashed line)), revealing the absence of any cathodic or anodic current responses. Afterward, a positive potential was applied at 0.800 V vs Ag|AgI|I^-, resulting in a large anodic current (Figure 6D) of ca. 7−8 mA. The stripping procedure was relatively fast, oxidizing all Cu^0 to Cu^{II} in less than 1 h, accompanied by a visual color change of the reaction medium to a clear green solution. Confirmation of our stripping procedure was accomplished by CV ((Figure 6D, inset (solid black line)) by the appearance of the characteristic Cu^{II}TPMA|Cu^{I}TPMA redox couple. Furthermore, UV−vis measurements and calculations based upon the Q confirmed a [Br−$Cu^{II}L^+$] of 1.07 mM and 1.02 mM, respectively, falling in close proximity to a theoretical [Br−$Cu^{II}L^+$] of 1.05 mM. Once the stripping procedure was completed, an identical polymerization was conducted to that of the first polymerization. The results of this second polymerization are shown in Figure 6A (green dots), illustrating nearly identical polymers can be obtained by utilizing the recycled copper catalyst.

CONCLUSION

This work serves as an extension of our initial work by providing systematic studies and evaluations of critical polymerization parameters from both an electrochemical and a polymerization standpoint. Polymerization rates were found to be correlated with η, whereby more negative potentials provide faster rates of polymerization and larger current values, until the system becomes mass transport limited. Higher $[Br-Cu^{II}L^+]_0$ yield faster rates of polymerization and larger current values, while simultaneously providing polymers with lower M_w/M_n values. More active catalyst systems resulted in faster rates of polymerization, larger current values, and lower M_w/M_n values. Control with less active catalyst complexes (i.e., with PMDETA ligand) could be gained upon using more positive potentials and higher $[Br-Cu^{II}L^+]_0$. Furthermore, the versatility of *e*ATRP was successfully demonstrated using various electrochemical methods: (a) galvanostatic conditions for simplified reaction setups and (b) copper deposition and stripping procedures for catalyst recycling/purification.

ASSOCIATED CONTENT

Supporting Information

Materials, instrumentation, methods, schemes, and supporting experimental results. This material is available free of charge via the Internet at http://pubs.acs.org.

AUTHOR INFORMATION

Corresponding Author

*E-mail: km3b@andrew.cmu.edu (K.M.).

Notes

The authors declare no competing financial interest.

ACKNOWLEDGMENTS

Financial support from the NSF (CHE 1026060) and the CRP Consortium at Carnegie Mellon University is greatly appreciated. The authors thank Mingjiang Zhong and Dr. Abdirisak A. Isse for their thoughtful discussions and comments.

REFERENCES

(1) Braunecker, W. A.; Matyjaszewski, K. *Prog. Polym. Sci.* **2007**, *32*, 93−146.
(2) (a) Moad, G.; Chong, Y. K.; Postma, A.; Rizzardo, E.; Thang, S. H. *Polymer* **2005**, *46*, 8458−8468. (b) Gregory, A.; Stenzel, M. H. *Prog. Polym. Sci.* **2012**, *37*, 38−105.
(3) (a) Hawker, C. J.; Bosman, A. W.; Harth, E. *Chem. Rev.* **2001**, *101*, 3661−3688. (b) Nicolas, J.; Guillaneuf, Y.; Lefay, C.; Bertin, D.; Gigmes, D.; Charleux, B. *Prog. Polym. Sci.* **2013**, *38*, 63−235.
(4) (a) Poli, R. *Angew. Chem., Int. Ed.* **2006**, *45*, 5058−5070. (b) Allan, L. E. N.; Perry, M. R.; Shaver, M. P. *Prog. Polym. Sci.* **2012**, *37*, 127−156.
(5) (a) Matyjaszewski, K.; Xia, J. *Chem. Rev.* **2001**, *101*, 2921−2990. (b) Kamigaito, M.; Ando, T.; Sawamoto, M. *Chem. Rev.* **2001**, *101*, 3689−3746. (c) Tsarevsky, N. V.; Matyjaszewski, K. *Chem. Rev.* **2007**, *107*, 2270−2299. (d) Matyjaszewski, K. *Macromolecules* **2012**, *45*, 4015−4039. (e) Siegwart, D. J.; Oh, J. K.; Matyjaszewski, K. *Prog. Polym. Sci.* **2012**, *37*, 18−37. (f) Matyjaszewski, K.; Tsarevsky, N. V. *Nat. Chem.* **2009**, *1*, 276−288. (g) Matyjaszewski, K.; Spanswick, J. In *Polymer Science: A Comprehensive Reference*; Matyjaszewski, K., Möller, M., Eds.; Elsevier BV: Amsterdam, 2012; Vol. 3, pp 377−428.
(6) di Lena, F.; Matyjaszewski, K. *Prog. Polym. Sci.* **2010**, *35*, 959−1021.
(7) De Paoli, P.; Isse, A. A.; Bortolamei, N.; Gennaro, A. *Chem. Commun.* **2011**, *47*, 3580−3582.
(8) (a) Tang, W.; Kwak, Y.; Braunecker, W.; Tsarevsky, N. V.; Coote, M. L.; Matyjaszewski, K. *J. Am. Chem. Soc.* **2008**, *130*, 10702−10713. (b) Magenau, A. J. D.; Kwak, Y.; Schröder, K.; Matyjaszewski, K. *ACS Macro Lett.* **2012**, *1*, 508−512.
(9) (a) Seeliger, F.; Matyjaszewski, K. *Macromolecules* **2009**, *42*, 6050−6055. (b) Braunecker, W. A.; Tsarevsky, N. V.; Gennaro, A.; Matyjaszewski, K. *Macromolecules* **2009**, *42*, 6348−6360. (c) Morick, J.; Buback, M.; Matyjaszewski, K. *Macromol. Chem. Phys.* **2012**, *213*, 2287−2292.
(10) (a) Jakubowski, W.; Matyjaszewski, K. *Angew. Chem., Int. Ed.* **2006**, *118*, 4594−4598. (b) Matyjaszewski, K.; Jakubowski, W.; Min, K.; Tang, W.; Huang, J.; Braunecker, W. A.; Tsarevsky, N. V. *Proc. Natl. Acad. Sci. U. S. A.* **2006**, *103*, 15309−15314.
(11) (a) Matyjaszewski, K.; Coca, S.; Gaynor, S. G.; Wei, M.; Woodworth, B. E. *Macromolecules* **1997**, *30*, 7348−7350. (b) Percec, V.; Guliashvili, T.; Ladislaw, J. S.; Wistrand, A.; Stjerndahl, A.; Sienkowska, M. J.; Monteiro, M. J.; Sahoo, S. *J. Am. Chem. Soc.* **2006**, *128*, 14156−14165. (c) Matyjaszewski, K.; Tsarevsky, N. V.; Braunecker, W. A.; Dong, H.; Huang, J.; Jakubowski, W.; Kwak, Y.; Nicolay, R.; Tang, W.; Yoon, J. A. *Macromolecules* **2007**, *40*, 7795−7806. (d) Magenau, A. J. D.; Kwak, Y.; Matyjaszewski, K. *Macromolecules* **2010**, *43*, 9682−9689. (e) Zhang, Y.; Wang, Y.; Peng, C.-h.; Zhong, M.; Zhu, W.; Konkolewicz, D.; Matyjaszewski, K. *Macromolecules* **2012**, *45*, 78−86.
(12) (a) Jakubowski, W.; Min, K.; Matyjaszewski, K. *Macromolecules* **2005**, *39*, 39−45. (b) Matyjaszewski, K.; Dong, H.; Jakubowski, W.; Pietrasik, J.; Kusumo, A. *Langmuir* **2007**, *23*, 4528−4531. (c) Li, B.; Yu, B.; Huck, W. T. S.; Zhou, F.; Liu, W. M. *Angew. Chem., Int. Ed.* **2012**, *51*, 5092−5095.
(13) Pietrasik, J.; Dong, H.; Matyjaszewski, K. *Macromolecules* **2006**, *39*, 6384−6390.
(14) (a) Rzayev, J.; Penelle, J. *Angew. Chem., Int. Ed.* **2004**, *43*, 1691−1694. (b) Kwiatkowski, P.; Jurczak, J.; Pietrasik, J.; Jakubowski, W.; Mueller, L.; Matyjaszewski, K. *Macromolecules* **2008**, *41*, 1067−1069.
(15) (a) Kwak, Y.; Matyjaszewski, K. *Macromolecules* **2010**, *43*, 5180−5183. (b) Tasdelen, M. A.; Uygun, M.; Yagci, Y. *Macromol. Chem. Phys.* **2011**, *212*, 2036−2042. (c) Mehmet Atilla, T.; Mustafa, Ç.; Mustafa, U.; Yusuf, Y. In *Progress in Controlled Radical Polymerization: Mechanisms and Techniques*; American Chemical Society: Washington, DC, 2012; Vol. *1100*, pp 59−72. (d) Fors, B. P.; Hawker, C. J. *Angew. Chem., Int. Ed.* **2012**, *51*, 8850−8853. (e) Konkolewicz, D.; Schröder, K.; Buback, J.; Bernhard, S.; Matyjaszewski, K. *ACS Macro Lett.* **2012**, *1*, 1219−1223.

(16) (a) Magenau, A. J. D.; Strandwitz, N. C.; Gennaro, A.; Matyjaszewski, K. *Science* **2011**, *332*, 81−84. (b) Bortolamei, N.; Isse, A. A.; Magenau, A. J. D.; Gennaro, A.; Matyjaszewski, K. *Angew. Chem., Int. Ed.* **2011**, *50*, 11391−11394.
(17) (a) Qiu, J.; Matyjaszewski, K.; Thouin, L.; Amatore, C. *Macromol. Chem. Phys.* **2000**, *201*, 1625−1631. (b) Kim, B. Y.; Ratcliff, E. L.; Armstrong, N. R.; Kowalewski, T.; Pyun, J. *Langmuir* **2009**, *26*, 2083−2092.
(18) (a) Hansen, T. S.; Lind, J. U.; Daugaard, A. E.; Hvilsted, S.; Andresen, T. L.; Larsen, N. B. *Langmuir* **2010**, *26*, 16171−16177. (b) Bonometti, V.; Labbé, E.; Buriez, O.; Mussini, P.; Amatore, C. *J. Electroanal. Chem.* **2009**, *633*, 99−105.
(19) (a) Hardy, C. G.; Ren, L. X.; Tamboue, T. C.; Tang, C. B. *J. Polym. Sci., Polym. Chem.* **2011**, *49*, 1409−1420. (b) Kraft, A.; Grimsdale, A. C.; Holmes, A. B. *Angew. Chem., Int. Ed.* **1998**, *37*, 402−428.
(20) (a) Tria, M. C. R.; Advincula, R. C. *Macromol. Rapid Commun.* **2011**, *32*, 966−971. (b) Nunige, S.; Cornut, R.; Hazimeh, H.; Hauquier, F.; Lefrou, C.; Combellas, C.; Kanoufi, F. *Angew. Chem., Int. Ed.* **2012**, *51*, 5208−5212. (c) Li, B.; Yu, B.; Huck, W. T. S.; Liu, W.; Zhou, F. *J. Am. Chem. Soc.* **2013**, *135*, 1708−1710.
(21) Bortolamei, N.; Isse, A. A.; Di Marco, V. B.; Gennaro, A.; Matyjaszewski, K. *Macromolecules* **2010**, *43*, 9257−9267.
(22) Bell, C. A.; Bernhardt, P. V.; Monteiro, M. J. *J. Am. Chem. Soc.* **2011**, *133*, 11944−11947.
(23) (a) Broderick, E. M.; Guo, N.; Vogel, C. S.; Xu, C. L.; Sutter, J.; Miller, J. T.; Meyer, K.; Mehrkhodavandi, P.; Diaconescu, P. L. *J. Am. Chem. Soc.* **2011**, *133*, 9278−9281. (b) Broderick, E. M.; Guo, N.; Wu, T. P.; Vogel, C. S.; Xu, C. L.; Sutter, J.; Miller, J. T.; Meyer, K.; Cantat, T.; Diaconescu, P. L. *Chem. Commun.* **2011**, *47*, 9897−9899. (c) Gregson, C. K. A.; Gibson, V. C.; Long, N. J.; Marshall, E. L.; Oxford, P. J.; White, A. J. P. *J. Am. Chem. Soc.* **2006**, *128*, 7410−7411.
(24) Isse, A. A.; Sandona, G.; Durante, C.; Gennaro, A. *Electrochim. Acta* **2009**, *54*, 3235−3243.
(25) Isse, A. A.; Gennaro, A. *J. Phys. Chem. A* **2004**, *108*, 4180−4186.
(26) (a) Bard, A. J.; Faulkner, L. R. *Electrochemical Methods: Fundamentals and Applications*, 2nd ed.; Wiley: New York, 2001. (b) Testa, A. C.; Reinmuth, W. H. *Anal. Chem.* **1961**, *33*, 1320−1324.
(27) Chan, N.; Cunningham, M. F.; Hutchinson, R. A. *Macromol. Chem. Phys.* **2008**, *209*, 1797−1805.
(28) Wang, Y.; Zhong, M.; Zhang, Y.; Magenau, A. J. D.; Matyjaszewski, K. *Macromolecules* **2012**, *45*, 8929−8932.